Galaxies in 3D across the Universe
Proceedings IAU Symposium No. 309, 2014
B. L. Ziegler, F. Combes, H. Dannerbauer, M. Verdugo, eds.

doi:10.1017/S1743921314009685

Dissecting galactic winds with the SAMI Galaxy Survey

I-Ting Ho[1] and the SAMI Galaxy Survey Team[2]

[1]Institute for Astronomy, University of Hawaii, 2680 Woodlawn Drive, Honolulu, HI 96822, USA
email: itho@ifa.hawaii.edu
[2]Full list of team members is available at http://sami-survey.org/members

Abstract. We conduct a case study on a normal star-forming galaxy ($z = 0.05$) observed by the SAMI Galaxy Survey and demonstrate the feasibility and potential of using large integral field spectroscopic surveys to investigate the prevalence of galactic-scale outflows in the local Universe. We perform spectral decomposition to separate the different kinematic components overlapping in the line-of-sight direction that causes the skewed line profiles in the integral field data. The three kinematic components present distinctly different line ratios and kinematic properties. We model the line ratios with the shock/photoionization code MAPPINGS IV and demonstrate that the different emission line properties are caused by major galactic outflows that introduce shock excitation in addition to photoionization. These results set a benchmark of the type of analysis that can be achieved by the SAMI Galaxy Survey on large numbers of galaxies.

Keywords. galaxies: evolution, galaxies: kinematics and dynamics - galaxies: starburst

1. Introduction

Galactic-scale outflows or galactic winds are one of the major "feedback" mechanisms regulating the mass assembly and star-forming activities of galaxies as they evolve over cosmic time (see Veilleux *et al.* 2005 for a review). Despite the import role outflows play in galaxy evolution, the prevalence and magnitudes of outflows are not well constrained. Observations of extra-planar optical emission and blue-shifted absorption lines have shown that starburst-driven winds are common in local galaxies ($z < 0.5$) with extreme star-forming activities with high star formation rate surface densities (e.g., $\Sigma_* \geqslant 0.1$ M$_\odot$ yr^{-1} kpc^{-2}, Heckman 2002; Rupke *et al.* 2005), and ubiquitous at high redshifts where the cosmic star formation rates peak (e.g., $z > 1.4$; Weiner *et al.* 2009; Steidel *et al.* 2010). For the normal star-forming population in the local Universe, detecting outflow signatures in individual galaxies are still difficult with the current spectroscopy surveys, unless with stacking analysis (e.g. Chen *et al.* 2010). Without spatially resolved data on a statistical sample, the prevalence and degree of galactic-scale outflows in normal star-forming galaxies remain largely unclear. The recent integral field spectroscopy survey using the new Sydney-AAO Multi-object Integral field spectrograph (SAMI; Croom *et al.* 2012) on the 3.9-m Anglo-Australian Telescope (i.e. the SAMI Galaxy Survey; Bryant *et al.* 2014; Allen *et al.* 2014) provides a unique opportunity to unravel the wind population in the local Universe ($z \lesssim 0.05$). In Ho *et al.* (2014), we demonstrate that by taking advantage of the high spectral resolution of SAMI (up to $R \approx 4500$) we can unambiguously identify wind galaxies through investigating the emission line ratios and kinematics. In this proceeding, some of the key results are summarized.

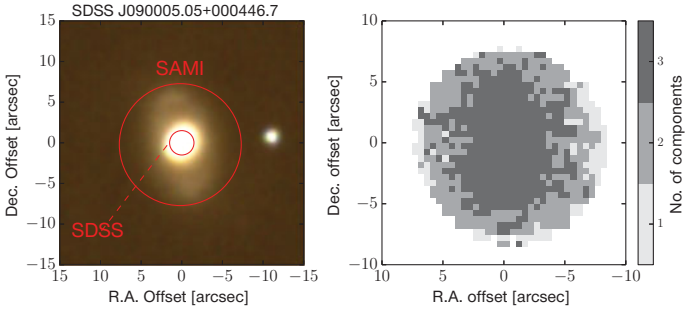

Figure 1. *Left:* SDSS *g, r, i* color composite image of SDSS J090005.05+000446.7 ($z = 0.05386$) over-plotted with footprints of Sloan Digital Sky Survey (SDSS) fiber and SAMI. The SDSS fiber has a diameter of 3″. The SAMI hexabundle has a circular field of view of 15″ in diameter. *Right:* Component map describing the number of components required to model the spectral profiles in each SAMI spaxel.

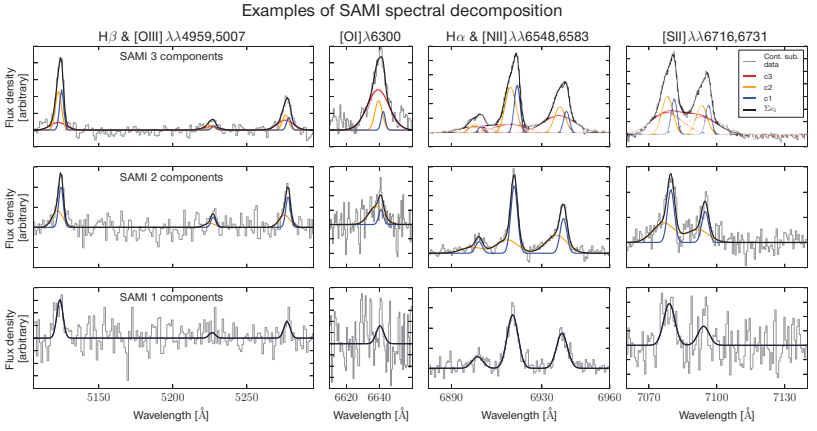

Figure 2. Examples of our spectral decomposition on selected spaxels requiring 3-component (top row), 2-component (middle row) and 1-component (bottom row) fits to describe the spectral profiles. Each panel shows a zoom-in of some key diagnostic emission lines. Continuum subtracted spectra are shown in grey. Best-fitting *c3*, *c2*, and *c1* are shown in red, orange, and blue, respectively. The best-fitting models, $\sum c_i$, are shown in black. To avoid confusion where the lines are blended, we also show individual line transitions of *c3* as transparent red lines.

2. Shocks and outflows in SDSS J090005.05+000446.7

In the integral field data of SDSS J090005.05+000446.7 (hereafter, SDSS J0900; left panel of Fig. 1) delivered by the SAMI Galaxy Survey, SDSS J0900 presents skewed line profiles changing with position in the galaxy because of the different kinematic components overlapping in the line-of-sight direction. We fit each spaxel with multiple component Gaussians depending on the complexity of the line profiles. In the most complicated cases, a broad *c3*, an intermediate *c2* and a narrow *c1* kinematic components are required to described the spectral profiles. Some examples of our spectral decomposition are shown in Fig. 2, and the right panel of Fig. 1 shows the numbers of components required at different locations in the SAMI field of view.

The different kinematic components present vastly different kinematic properties (see Ho *et al.* 2014) and line ratios. On the classical BPT diagrams (top row of Fig. 3), the emission line ratios of the different components are distinctly different, with the narrow *c1* component consistent with photoionization, the broad *c3* component consistent

https://doi.org/10.1017/S1743921314009685 Published online by Cambridge University Press

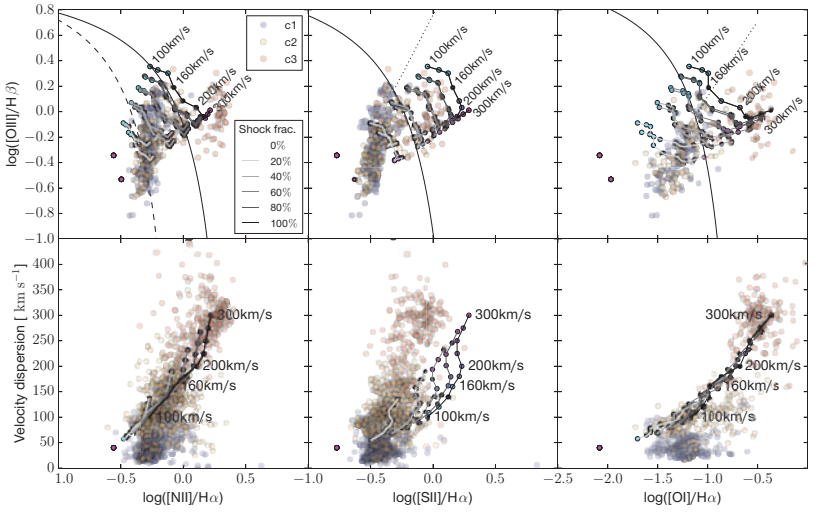

Figure 3. *Top row:* The three classical BPT diagrams (Baldwin *et al.* 1981). *Bottom row:* The three key line ratios versus velocity dispersion. The blue, orange, and red points correspond to the different kinematic components (see Fig. 2). The other color points connected by line segments are shock/photoionization model grids from `MAPPINGS` (see Ho *et al.* 2014 for details). The line segments connect model grids of certain shock fractions with changing shock velocities. The pure photoionization points (zero shock fraction) are at the bottom left corners (magenta). The different components show distinctly different line ratios and kinematics and the `MAPPINGS` models well reproduce the observations.

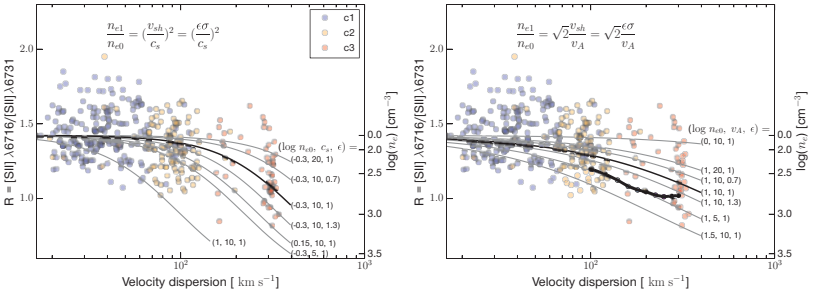

Figure 4. [S II] ratios and electron densities, versus velocity dispersion. The curves are models of isothermal shocks propagating in ISM without magnetic field (left panel) and with magnetic field (right panel). The models providing the best representation of the data are shown as the black curves. The models with different parameters close to those of the black models are shown in grey. The three parameters adopted in each model are labeled next to each curve. The units are cm^{-3} for the pre-shock electron density (n_{e0}), and km s^{-1} for the sound speed (c_s) and Alfvén velocity (v_A). The geometric factor (ϵ) is unit-less. The predictions from the MAPPINGS IV shock models are shown as thick black segments in the right panel.

with low-ionization narrow emission-line regions, and the intermediate *c2* component presenting intermediate line ratios. Clear correlations between the line ratios and velocity dispersion are also obvious in the bottom row of Fig. 3. We model the line ratios using the shock/photoionization code MAPPINGS (Sutherland & Dopita 1993; Dopita & Sutherland 1996; Allen *et al.* 2008; Dopita *et al.* 2013), and we reach remarkable agreement between the data and the models. The elevated line ratios and velocity dispersion of the broad *c3* component are due to the presence of interstellar shocks ($v \approx$ 200–300 km s^{-1}) induced by the galactic winds in SDSS J0900. The models demonstrate that the narrow

https://doi.org/10.1017/S1743921314009685 Published online by Cambridge University Press

c1 component is excited by pure photoionization originated from star-forming regions on the disk, and the intermediate *c2* component is excited by a combination of both photoionization and shock excitation.

The presence of interstellar shocks also directly result in the compression of gas, causing the elevation of electron density traceable with the density sensitive line ratio [S II] λ6716/[S II] λ6731. The degrees of compression are related to the shock velocities. The elevated electron densities of the broad *c3*, shock-excited component are both observed in our data and consistent with the inferred shock velocities of 200–300 km s^{-1}. Fig. 4 shows two scenarios where the shocks travel in non-magnetized (left panel) and magnetized (right) medium. The high electron densities of *c3* are consistent with the model predictions, demonstrating the importance of shock excitation and the presence of major galactic winds in SDSS J0900.

3. Conclusions

We present the key features to investigate in high-resolution integral field data when major galactic-scale outflows occur. While this case study poses no immediate answer to the prevalence of galactic winds in the local Universe, the large sample size (final sample size of 3,400 galaxies) of the SAMI Galaxy Survey will soon enable an array of studies on galactic-scale outflows and winds in the local Universe (e.g. Fogarty *et al.* 2012).

Acknowledgements

This research makes use of the data products from the SAMI Galaxy Survey†.

References

Allen, J. T., Croom, S. M., Konstantopoulos, I. S., *et al.* 2014, ArXiv e-prints, arXiv:1407.6068

Allen, M. G., Groves, B. A., Dopita, M. A., Sutherland, R. S., & Kewley, L. J. 2008, *ApJS*, 178, 20

Baldwin, J. A., Phillips, M. M., & Terlevich, R. 1981, *PASP*, 93, 5

Bryant, J. J., Owers, M. S., Robotham, A. S. G., *et al.* 2014, ArXiv e-prints, arXiv:1407.7335

Chen, Y.-M., Tremonti, C. A., Heckman, T. M., *et al.* 2010, *AJ*, 140, 445

Croom, S. M., Lawrence, J. S., Bland-Hawthorn, J., *et al.* 2012, *MNRAS*, 421, 872

Dopita, M. A. & Sutherland, R. S. 1996, *ApJS*, 102, 161

Dopita, M. A., Sutherland, R. S., Nicholls, D. C., Kewley, L. J., & Vogt, F. P. A. 2013, *ApJS*, 208, 10

Fogarty, L. M. R., Bland-Hawthorn, J., Croom, S. M., *et al.* 2012, *ApJ*, 761, 169

Heckman, T. M. 2002, in Astronomical Society of the Pacific Conference Series, Vol. 254, Extragalactic Gas at Low Redshift, ed. J. S. Mulchaey & J. T. Stocke, 292

Ho, I.-T., Kewley, L. J., Dopita, M. A., *et al.* 2014, *MNRAS*, in press (arXiv:1407.2411)

Rupke, D. S., Veilleux, S., & Sanders, D. B. 2005, *ApJS*, 160, 115

Steidel, C. C., Erb, D. K., Shapley, A. E., *et al.* 2010, *ApJ*, 717, 289

Sutherland, R. S. & Dopita, M. A. 1993, *ApJS*, 88, 253

Veilleux, S., Cecil, G., & Bland-Hawthorn, J. 2005, *ARA&A*, 43, 769

Weiner, B. J., Coil, A. L., Prochaska, J. X., *et al.* 2009, *ApJ*, 692, 187

† The SAMI Galaxy Survey is based on observation made at the Anglo-Australian Telescope. The Sydney-AAO Multi-object Integral field spectrograph was developed jointly by the University of Sydney and the Australian Astronomical Observatory. The SAMI input catalogue is based on data taken from the Sloan Digital Sky Survey, the GAMA Survey and the VST ATLAS Survey. The SAMI Galaxy Survey is funded by the Australian Research Council Centre of Excellence for All-sky Astrophysics, through project number CE110001020, and other participating institutions. The SAMI Galaxy Survey website is `http://sami-survey.org/`.